







# Intrinsic cancer cell phosphoinositide 3-kinase $\delta$ regulates fibrosis and vascular development in cholangiocarcinoma

Vanessa Bou Malham<sup>1,2</sup>  | Nassima Benzoubir<sup>1,2</sup> | Javier Vaquero<sup>3,4</sup> | Christophe Desterke<sup>5</sup> | Jean Agnetti<sup>1,2</sup> | Pei Xuan Song<sup>1,2</sup> | Ester Gonzalez-Sanchez<sup>3,6,7,8</sup>  | Ander Arbelaz<sup>3</sup> | Sophie Jacques<sup>9</sup> | Emanuel Di Valentin<sup>10</sup> | Souad Rahmouni<sup>9</sup> | Tuan Zea Tan<sup>11</sup> | Didier Samuel<sup>1,2,12</sup>  | Jean Paul Thiery<sup>13</sup> | Mylène Sebah<sup>1,2,14</sup>  | Laura Fouassier<sup>3</sup>  | Ama Gassama-Diagne<sup>1,2</sup> 

<sup>1</sup>INSERM, Unité 1193, Villejuif, France

<sup>2</sup>Université Paris-Saclay, UMR-S 1193, Villejuif, France

<sup>3</sup>Centre de Recherche Saint-Antoine, CRSA, Sorbonne Université, INSERM, Paris, France

<sup>4</sup>Centro de Investigación del Cáncer, Instituto de Biología Molecular y Celular del Cáncer, CSIC-Universidad de Salamanca, Salamanca, Spain

<sup>5</sup>Université Paris-Saclay, UFR Médecine-INSERMS1310, Villejuif, France

<sup>6</sup>TGF- $\beta$  and Cancer Group, Oncobell Program, Bellvitge Biomedical Research Institute (IDIBELL), Barcelona, Spain

<sup>7</sup>Oncology Program, CIBEREHD, National Biomedical Research Institute on Liver and Gastrointestinal Diseases, Instituto de Salud Carlos III, Madrid, Spain

<sup>8</sup>Inovarian, Paris, France

<sup>9</sup>Laboratory of Animal Genomics, GIGA-Medical Genomics, GIGA-Institute, University of Liège, Liège, Belgium

<sup>10</sup>Plateforme des vecteurs viraux, Université de Liège, GIGA B34, Liège, Belgium

<sup>11</sup>Genomics and Data Analytics Core (GeDaC), Cancer Science Institute of Singapore, National University of Singapore, Singapore, Singapore

<sup>12</sup>Centre Hepato-Biliaire, AP-HP Hôpital Paul Brousse, Villejuif, France

<sup>13</sup>Guangzhou Laboratory, International Biological Island Guangzhou, Guangzhou, China

<sup>14</sup>Laboratoire d'Anatomopathologie, AP-HP Hôpital Paul-Brousse, Villejuif, France

## Correspondence

Ama Gassama-Diagne, Centre Hépatologie-Biliaire, Inserm UMRS-1193, Hôpital Paul Brousse, 12 Avenue Paul Vaillant Couturier, Villejuif 94807, Cedex, France.  
Email: [ama.gassama@inserm.fr](mailto:ama.gassama@inserm.fr)

## Funding information

ITMO Cancer of Aviesan; Inserm, Grant/Award Number: ANR-17-CE14-0013-01 and INCa\_16428; Fondation pour la Recherche Médicale, Grant/Award Number: SPF201809007054 and EQU202003010517; Les Entreprises contre le Cancer Paris – Île-de-France; Spanish Association for the Study of the Liver (AEEH); Fondation ARC, Grant/

## Abstract

**Background & Aims:** The class I- phosphatidylinositol-3 kinases (PI3Ks) signalling is dysregulated in almost all human cancers whereas the isoform-specific roles remain poorly investigated. We reported that the isoform  $\delta$  (PI3K $\delta$ ) regulated epithelial cell polarity and plasticity and recent developments have heightened its role in hepatocellular carcinoma (HCC) and solid tumour progression. However, its role in cholangiocarcinoma (CCA) still lacks investigation.

**Approach & Results:** Immunohistochemical analyses of CCA samples reveal a high expression of PI3K $\delta$  in the less differentiated CCA. The RT-qPCR and immunoblot analyses performed on CCA cells stably overexpressing PI3K $\delta$  using lentiviral construction reveal an increase of mesenchymal and stem cell markers and the pluripotency

**Abbreviations:** bFGF, basic fibroblast growth factor; CAFs, cancer-associated fibroblasts; CCA, cholangiocarcinoma; CK19, cytokeratin 19; eCCA, extrahepatic CCA, CSCs, Cancer stem cells; ECM, extracellular matrix; EMT, epithelial to mesenchymal transition; EpCAM, epithelial cell adhesion molecules; GO-BP, gene ontology biological process; HCC, hepatocellular carcinoma; iCCA, intrahepatic CCA; MDCK, Madin-Darby canine kidney; pCCA, Perihilar CCA; PI3K, phosphoinositide 3-kinase; PIGF, placental growth factor; TGF $\beta$ , transforming growth factor beta; TMA, tissue microarray; VEGF-A, vascular endothelial growth factor A; VEGF-C, vascular endothelial growth factor C.

This is an open access article under the terms of the [Creative Commons Attribution-NonCommercial-NoDerivs](https://creativecommons.org/licenses/by-nc-nd/4.0/) License, which permits use and distribution in any medium, provided the original work is properly cited, the use is non-commercial and no modifications or adaptations are made.

© 2023 The Authors. *Liver International* published by John Wiley & Sons Ltd.

Award Number: PDF2014601431; LABEX PLAS@PAR, Grant/Award Number: ANR-11-IDEX-0004-02; Spanish Ministry for Science and Innovation, Grant/Award Number: RYC2021-034121-I; EURO-CHOLANGIO-NET, Grant/Award Number: CA18122; La Ligue contre le Cancer

Handling Editor: Alejandro Forner

transcription factors. CCA cells stably overexpressing PI3K $\delta$  cultured in 3D culture display a thick layer of ECM at the basement membrane and a wide single lumen compared to control cells. Similar data are observed *in vivo*, in xenografted tumours established with PI3K $\delta$ -overexpressing CCA cells in immunodeficient mice. The expression of mesenchymal and stemness genes also increases and tumour tissue displays necrosis and fibrosis, along with a prominent angiogenesis and lymphangiogenesis, as in mice liver of AAV8-based-PI3K $\delta$  overexpression. These PI3K $\delta$ -mediated cell morphogenesis and stroma remodelling were dependent on TGF $\beta$ /Src/Notch signalling. Whole transcriptome analysis of PI3K $\delta$  using the cancer cell line encyclopedia allows the classification of CCA cells according to cancer progression.

**Conclusions:** Overall, our results support the critical role of PI3K $\delta$  in the progression and aggressiveness of CCA via TGF $\beta$ /src/Notch-dependent mechanisms and open new directions for the classification and treatment of CCA patients.

#### KEYWORDS

EMT, extracellular-matrix, stemness, tumour growth, vasculature development

## 1 | INTRODUCTION

CCA is a highly heterogeneous cancer of the biliary tract, which is classified into intrahepatic (iCCA), occurring in the intrahepatic bile ducts, perihilar (pCCA) and distal extrahepatic (dCCA) bile duct cancers.<sup>1</sup> iCCA represents the second most frequent type of primary liver cancer after hepatocellular carcinoma (HCC). CCA has a poor survival rate, a high recurrence and a rising global incidence.<sup>2</sup> Unfortunately, due to late diagnosis, only few patients are eligible for surgery which remains the only effective therapeutic option.<sup>2</sup> Thus, the clinical management of patients with CCA is still a challenge.

The CCA is considered as a tumour originated from the cholangiocytes, the epithelial cells lining bile ducts, while HCC is derived from hepatocytes.<sup>3,4</sup> However, emerging literature revealed a more complicated scenario. Indeed, hepatocytes and cholangiocytes are virtually quiescent in healthy adult liver but exhibit a remarkable plasticity following severe injury, allowing these cells to dedifferentiate or transdifferentiate and acquire stem cell traits, thus contributing to both HCC and CCA with recurrence and resistance to treatment.<sup>5</sup> The most studied form of cellular plasticity is the epithelial to mesenchymal transition (EMT), a process through which epithelial cells lose their polarity and differentiation traits to acquire mesenchymal, then invasive characteristics.<sup>6</sup> EMT and its reverse process mesenchymal-epithelial transition (MET) represent key mechanisms in embryonic development and are essential driver of plasticity in cancer.<sup>7-9</sup>

The most frequently deregulated enzymes in cancer are the class I phosphoinositide 3-kinases (PI3Ks)<sup>10</sup> which consist of four isoforms ( $\alpha$   $\beta$   $\gamma$   $\delta$ ). Pan-PI3K inhibitors were used in most of the fundamental and clinical studies to decipher their numerous biological functions while the isoform-specific roles just started to be investigated.<sup>11,12</sup> The isoform  $\delta$  (PI3K $\delta$ ) is the last

#### Key points

The cholangiocarcinoma is a highly aggressive liver cancer with poor survival rate, a high recurrence and a rising global incidence. Unfortunately, due to late diagnosis and effective therapeutic option, the clinical management of patients with CCA is still a challenge. We identified here a new target for diagnosis and treatment and our data also opened new directions for classification and treatment of patients.

identified member of class I of the PI3Ks and is mostly expressed in the spleen and thymus.<sup>13</sup> Although the PI3K $\delta$  inhibitor idelalisib (Zydelig/CAL-101) became the first PI3K inhibitor to be approved for the treatment of leukaemia and lymphoma,<sup>14,15</sup> a role for PI3K $\delta$  in non-hematopoietic cells was under investigated in part due to its low expression in different tissues. Nonetheless, recent reports described elevated expression of PI3K $\delta$  in different cancers including breast cancer,<sup>16,17</sup> colon cancer<sup>18</sup> and HCC<sup>19,20</sup> while none of these studies concerned CCA.

The CCA is characterized by a dense, reactive desmoplastic stroma marked by a dramatic accumulation of extracellular matrix (ECM).<sup>21</sup> We reported a key role of PI3K $\delta$  in apico-basal polarity and particularly in the lumen formation and the assembly of ECM at the basement membrane using 3D culture of CCA cells.<sup>22</sup> We recently showed that activity of PI3K $\delta$  discriminates stemness from EMT, representing a crucial regulator of hepatocyte plasticity.<sup>30</sup> In this study, we sought to determine the expression and the potential role of PI3K $\delta$  in CCA tumour cell plasticity and its impact *in vivo* on the tumour growth and the remodelling of the stroma.

## 2 | METHODS

### 2.1 | CCA cell lines and culture media

HuCCT-1 cells, derived from the intrahepatic biliary tract, were kindly provided by Dr. G. Gores (Mayo Clinic, MN). CC-LP-1, SG-231 and Huh-28 cells, derived from the intrahepatic biliary tract were kindly provided by Dr. Cédric Coulouarn (Inserm U1242 'Oncogenesis, stress, Signaling' (OSS)). EGI-1 cells, established from the advanced stage of primary bile duct carcinoma, were obtained from the German Collection of Microorganisms and Cell Cultures (DSMZ). SK-ChA-1 and Mz-ChA-1 cells, derived from extrahepatic CCA (eCCA), were obtained from Dr. A. Knuth (Zurich University). EGI-1, HuCCT-1, Mz-ChA-1 and SK-ChA-1 cells were cultured in DMEM supplemented with 1 g/L glucose, 1% HEPES, 10% fetal bovine serum (FBS) and 1% penicillin. CC-LP-1 and Huh7 cells were cultured in DMEM supplemented with 4.5 g/L glucose, 10% FBS, 1% penicillin, 1% MEM NEAA and 1% sodium pyruvate. Huh-28 cells were cultured in MEM supplemented with 10% FBS and 1% penicillin. SG-231 cells were cultured in MEM supplemented with 10% FBS, 1% penicillin and 10 mmol/L HEPES. All cell lines were routinely screened for the presence of mycoplasma. PI3K $\delta$  inhibitor, idelalisib (Zydelig/CAL-101) was purchased from Selleckchem. Stable PI3K $\delta$  expression in EGI-1 and HuCCT-1 cells was performed using lentiviral vectors.

The EMT score for each cell line was calculated using the transcriptome data from cancer cell line encyclopedia (CCLE) database as reported.<sup>34</sup>

### 2.2 | PI3K $\delta$ overexpression stable CCA cell models

Plasmid containing the coding sequence for a fusion protein PI3K $\delta$ -mCherry or the corresponding control mCherry alone (under CMV promoter) were used to generate  $\Delta$ U3 SIN lentiviral vectors (rLVs). These rLVs were generated by the GIGA Viral Vectors platform. Briefly Lenti-X 293T cells (Clontech®, 632180) were co-transfected with a pSPAX2 (Addgene®) and a VSV-G encoding vector.<sup>23</sup> Culture supernatants, containing rLV, were collected 48, 72 and 96 h post-transfection, filtrated (0.2  $\mu$ m) and concentrated 100  $\times$  by ultracentrifugation. The rLVs were then titrated with qPCR Lentivirus Titration (Titre) Kit (ABM®, LV900). Briefly, CCA cells (EGI-1 and HuCCT1) were transduced (using 50 rLV/cells) and maintained in the presence of rLV for 24 h. Then, rLVs were eliminated and fresh media was added to maintain cells in culture for another 48 h until mCherry expression was observed. Positive transduced cells were detected by positive fluorescence signal and they were selected by treatment with lethal doses of puromycin for 72 h to eliminate non-transduced cells.

### 2.3 | 3D culture

The eight-well Lab-Tek II chamber slides (Thermo Fisher Scientific) were coated with Matrigel, then added with 10000 cells/well in 2% Matrigel (BD Biosciences) and grown for up to 6 days.

### 2.4 | Immunoblot

Cells were isolated using Laemmli buffer, then denatured at 95°C for 5 min. Protein samples were separated using 10% SDS-PAGE and then transferred onto a nitrocellulose blotting membrane (Amersham Protran). After blocking in 5% milk in TBST, primary antibodies were added at 4°C overnight. The membrane was put into appropriate secondary antibodies coupled with peroxidase under room temperature. Protein bands were visualized with chemiluminescent peroxidase substrate (Chemiluminescent Peroxidase Substrate-3; Sigma-Aldrich) and exposure using Gbox. The antibodies used are indicated in Table S2.

### 2.5 | Quantitative reverse transcription-PCR

RNeasy Mini Kit 50 (Qiagen) was used to extract total RNA, with the RevertAid First Strand cDNA Synthesis Kit (ThermoFisher) for reverse transcription. The Quanti Tect SYBR Green PCR Kit (Qiagen) was used for qPCR reactions using a LightCycler® 96 Instrument (Lifescience, Roche) following these parameters: 50°C for 30 min, 95°C for 15 min, followed by 40 cycles of 94°C for 30 s, 55°C for 30 s and 72°C for 30 s. The primers used in this study are provided in Table S3.

### 2.6 | Colony formation assay

CCA cells were seeded as 200 cells/well in a 6-well plate in a low attached and then cultured for 7 days. Colonies were fixed and stained with a 0.5% crystal violet solution.

### 2.7 | Transcriptomic dataset

The analysis of transcriptomic gene expression was performed on liver cancer samples (Woo et al., 2010) using Affymetrix Human Genome U133A 2.0 Array technology that was downloaded from the Geo Omnibus Database. An RMA Normalized Gene expression matrix from the GSE15765 dataset was annotated with the GEO platform file GPL571 by means of an SQL query.

### 2.8 | Cancer cell line encyclopedia RNA-sequencing

Through cancer dependency map (depmap) data webportal (<https://depmap.org/portal/>), it was possible to access the next-generation sequencing characterization of 1072 cell lines from Cancer Cell Line Encyclopedia (CCLE).<sup>24</sup> With cell line selector 26 cancer lines derived intrahepatic cholangiocarcinoma were selected to perform scatterplot analysis between expression of *VIM* and *PIK3CD*. Downstream bioinformatics analyses

were performed in R software environment version 4.1.3. Total RNA-sequencing data of the 26 iCCA cell lines were downloaded and upper quantile normalized with NOISeq R-package version 2.36.0<sup>25</sup> (Figure S11A,B). VIM-PIK3CD dependent expression signature was determined by supervised machine learning based on leaving one cross-validation process with pamr R-package version 1.56.1.<sup>26</sup> Unsupervised principal component analysis was done with 'prcomp' R base function and drawn with the autoplot function of ggfortify R-package version 0.4.14. Expression heatmaps were drawn with pheatmap R-package version 1.0.12 with clustering on Euclidean distances. Geneset functional enrichments were performed with Toppgene web application<sup>27</sup> on Gene Ontology database.<sup>28</sup> Functional enrichment networks were drawn with Cytoscape standalone application version 3.6.0.<sup>29</sup>

## 2.9 | Xenograft tumour model

Animal experiments were performed in accordance with the French Animal Research Committee guidelines and all procedures were approved by a local ethics committee (No 01346.02). Cells ( $2 \times 10^6$ ) suspended in 60  $\mu$ L of PBS were mixed with 60  $\mu$ L of Matrigel growth factor reduced (Corning) and implanted subcutaneously into the flank of 5-week-old female NMRI-nu (nu/nu) mice. Mice were housed under standard conditions in individually ventilated cages enriched with a nesting material and kept at 22°C on a 12-h light/12-h dark cycle with ad libitum access to food and tap water. Tumour growth was followed with a calliper and tumour volume (V) was calculated as follows: xenograft volume =  $xy^2/2$  where x is the longest and y is the shortest of two perpendicular diameters. Mz-ChA-1, HuCCT-1, CCLP-1, EGI-1-Control-mCherry and EGI-1-PI3K $\delta$ -mCherry were injected and the mice were maintained until tumours reached a volume of 1000 mm<sup>3</sup>. During the experiment, animals showed no sign of toxicity, such as body weight loss (>15%), decreased food intake or diarrhoea. On the day of the sacrifice, a slice of the tumour was fixed in 10% formalin and embedded in paraffin, and the rest was cut in pieces and frozen in liquid nitrogen for further analysis.

## 2.10 | Histology and immunohistochemistry of xenografts

The hepatic tumours selected for inclusion in a tissue microarray (TMA) were obtained from the 'Centre de Ressources Biologiques Paris-Sud', Paris-Sud University, Villejuif, France. Access to this material was in agreement with French legislation. Tissue samples were collected at the time of surgical resection with the prior informed consent of patients. The local research ethics committee specifically approved this procedure. All cases were reviewed by a pathologist.

Tissue sections fixed in formalin (4%) and paraffin-embedded, 4  $\mu$ m thick, were deparaffinized with Ottix Plus and Ottix Shaper

(DIAPATH), and stained either with haematoxylin and eosin or Sirius red. For immunohistochemistry, antigens were unmasked with citrate buffer pH8. Sections were incubated sequentially with H<sub>2</sub>O<sub>2</sub> for 5 min, with Protein Block (Novolink Polymer Detection System; Novocastra Laboratories, Ltd.) for 5 min, and with primary antibodies for 30 min or overnight (CK19, CD31, PI3K $\delta$ ). Novolink Post Primary was applied for 15 min. Sections were finally washed and incubated with Novolink Polymer for 15 min or anti-rat HRP for 1 h (for CK19, CD31, PI3K $\delta$ ). All immunohistochemical staining results were analysed by an expert in liver pathology (MS). The intensity of the signal was quantified using the 'image J' software. The antibodies used are described in Tables S2 and S4.

## 2.11 | Immunofluorescence staining

The cells grown in matrigel or on coverslips and tissue sections embedded in paraffin were washed with ice-cold Dulbecco's PBS (DPBS) and fixed with 4% paraformaldehyde at 4°C for 20 min. After washing twice using DPBS, the tissue sections were deparaffinized with Ottix Plus and Ottix Shaper (DIAPATH) as described above for immunohistochemistry. The fixed cells or tissue sections were permeabilized and saturated with DPBS supplemented with 0.7% fish gelatin and 0.025% saponin for 30 min at 37°C, then incubated with the primary antibodies. After washing, incubation was performed with the secondary fluorescent antibodies and Hoechst. Leica TCS SP5 AOBs tandem 30 confocal microscope was used for image acquisition and analysis using Fiji/ImageJ, 1.48v.

## 2.12 | AAV-2/8 vectors production and mice lentiviral transduction

Mouse PI3K $\delta$  expression in the liver was achieved by AAV gene transfer plasmids pAAV TBG m PI3K $\delta$  (VB180205-1022wdw, Vector Builder) according to the previous study.<sup>30</sup> 8-week-old C57BL/6 mice (purchased from Charles River) were injected in the tail vein using pAAV TGB m PI3K $\delta$  and pAAV TBG EGFP adenovirus ( $10^{11}$  particules/mouse). Eight weeks later, mice were sacrificed. The mouse liver was divided into parts: one lobe was fixed in 4% formalin for 24 h and embedded in paraffin for further immunohistochemistry staining; the rest of the liver was snap-frozen and kept at -80°C for RNA extraction and RT-qPCR analyses.

## 2.13 | Statistical analysis

All values are expressed as mean  $\pm$  SEM. Comparisons of mean values were performed using an unpaired Student's *t* test except when mentioned in legend.

### 3 | RESULTS

#### 3.1 | PI3K $\delta$ expression in liver cancers is related to pluripotent stem cell markers and EMT markers

We investigated the expression of PI3K $\delta$  in primary liver cancers HCC ( $n=70$ ), mixed ( $n=7$ ) and iCCA ( $n=13$ ) using the transcriptomic dataset GSE15765. We found that PI3K $\delta$  (*PI3KCD*) expression was the highest in iCCA compared to the mixed HCC-iCCA and HCC (Figure 1A). Furthermore, in these liver cancers, we found a positive correlation between PI3K $\delta$  expression and cytokeratin 19 (*KRT19*), a marker of CCA (Figure 1B). Most of all, PI3K $\delta$  expression was highly correlated with the pluripotency (*SOX2*, *POU5F1* and *NANOG*) and CSC markers (*CD44*, *CD133* and *CD90*) (Figure 1B).

We then assessed the PI3K $\delta$  expression in liver biopsies samples using a tissue microarray as previously described.<sup>31</sup> Data from 19 samples of patients with iCCA, 16 samples of pCCA and 9 samples of HCC revealed a high expression of PI3K $\delta$  in iCCA and pCCA, compared to HCC (Figure 1C). The PI3K $\delta$  expression was the highest in the moderately differentiated iCCA compared to the well-differentiated tumours (Figure 1C–F).

Together these data strongly suggested that increased PI3K $\delta$  expression could promote dedifferentiation of CCA cells and induce stemness.

#### 3.2 | PI3K $\delta$ expression in CCA cells increases mesenchymal and CSC markers

To evaluate the role of PI3K $\delta$  in CCA, we used human CCA cell lines from different origins as mentioned in methods and including Mz-ChA-1, EGI-1, HuCCT1, SK-ChA-1, SG-231, Huh28, CCLP1. The cells were classified according to their EMT scores<sup>34</sup> and we evaluated the PI3K $\delta$  expression and that of two classical EMT markers, the E-Cadherin and vimentin as epithelial and mesenchymal proteins respectively. PI3K $\delta$  expression was almost no detectable in the cells with the highest epithelial features such as Mz-ChA-1 and EGI-1 whereas its expression was very high in Huh28 and CCLP1 enriched in vimentin and thus more mesenchymal (Figure 2A). Similar data were obtained using RT-qPCR (Figure S1). Strikingly these results showed that expression of PI3K $\delta$  was correlated with EMT. Given that EMT plays a critical role in the acquisition of stemness by cancer cells<sup>9</sup> and our recent report that demonstrated the role of PI3K $\delta$  in EMT and stemness,<sup>35</sup> we performed colony forming assay in six among these CCA cells and results supported that high PI3K $\delta$  expression is associated with increase self-renewal capacity (Figure 2B). Subsequently, EGI-1 CCA cells were transduced with either the lentivirus coding PI3K $\delta$ -mCherry construct (EGI-1-PI3K $\delta$ ) or mCherry-tag (EGI-1) to establish stable cell lines and the increased PI3K $\delta$  protein and *PI3KCD* mRNA levels validated (Figure 2C). Interestingly, PI3K $\delta$  overexpression exhibited increased self-renewal capacity of these cells, confirmed by colony forming assay (Figure 2D). In addition,

we verified that PI3K $\delta$  overexpression increased the epithelial markers (CK19, E-cadherin), mesenchymal markers (CD90, CD44, vimentin, N-cadherin, ZEB1), pluripotency markers (Sox2, Nanog, Oct-4) (Figure 2E) and several TGF $\beta$ /Src signalling markers (Src, TGF $\beta$ , SMAD7) in EGI-1-PI3K $\delta$  cells (Figure 2F). We also showed an increase in *PIK3CD* expression in EGI-1 cells were treated with 2 doses of TGF $\beta$  (Figure 2F). These data are in line with our recent report using HCC-derived Huh7 cells overexpressing PI3K $\delta$ .<sup>35</sup> We validated the increased vimentin and Nanog expressions by immunofluorescence staining (Figure 2G).

To validate these data, HuCCT-1 cells were transduced with either the lentivirus coding PI3K $\delta$ -mCherry construct (HuCCT-1-PI3K $\delta$ ) or mCherry-tag (HuCCT-1) (Figure S2) similarly to EGI-1. Interestingly, we observed obtained similar data in HuCCT-1-PI3K $\delta$  cells (Figure S2A–D). Taken together these results suggested a role of PI3K $\delta$  in the aggressiveness of CCA cells, related to stemness and EMT and potentially through activation of TGF $\beta$ /Src signalling.

#### 3.3 | PI3K $\delta$ promotes CCA tumour growth by stimulating fibrosis and angiogenesis via TGF $\beta$

The tumour growth ability of four different CCA cell lines in xenograft models was evaluated, and a correlation between PI3K $\delta$  expression in CCA cells and the tumour growth rate was observed in all of them (Figure S3). Thus, to explore the role of PI3K $\delta$  in CCA development in vivo, the EGI-1-PI3K $\delta$  cells were also engrafted in immunocompromised mice (Figure 3A). The overexpression of PI3K $\delta$  in EGI-1 cells validated by RT-qPCR (Figure S4A), significantly increased the tumour growth rate which reached a volume of 1000 mm<sup>3</sup> in <45 days and a higher tumour weight compared to control (Figure 3B). The histology of xenografts showed that EGI-1 cells recapitulated all the features of likely differentiated CCA with a glandular structure and limited necrosis (Figure 3C and Figure S4B). The necrosis for the different xenograft samples was presented in Figure S4B. Immunohistochemistry staining of the tumours revealed a rise of CK19 expression in xenografts from EGI-1-PI3K $\delta$  (Figure 3C) accompanied by an up-regulation of CK19 mRNA level (Figure 3D). Picrosirius red staining showed an expanded fibrosis area with an increase in PI3K $\delta$  expression (Figure 3C). Unexpectedly CD31 strongly increased in xenografts from EGI-1-PI3K $\delta$  cells (Figure 3C) and thus indicated a potential role of PI3K $\delta$  in angiogenesis. Furthermore, the human *COL4A4* and fibronectin (*FN1*) instead of mouse *FN1* were increased in the presence of PI3K $\delta$  (Figure 3D). The cancer-associated fibroblasts (CAFs) play a key role in fibrosis and EMT. Nevertheless, mouse *Acta2*/ $\alpha$ -smooth muscle actin ( $\alpha$ SMA) used to quantify the CAFs and *Adgre1*/F4/80, used to quantify the tumour-associated macrophages (TAM) did not significantly change (Figure 3D). Thus, these data suggested that the increased fibrosis and angiogenesis were controlled by the implanted human EGI-1-PI3K $\delta$  cells. To get insights into the mechanisms involved in the profound effects induced by PI3K $\delta$  expression in EGI-1-PI3K $\delta$  tumour, we investigated

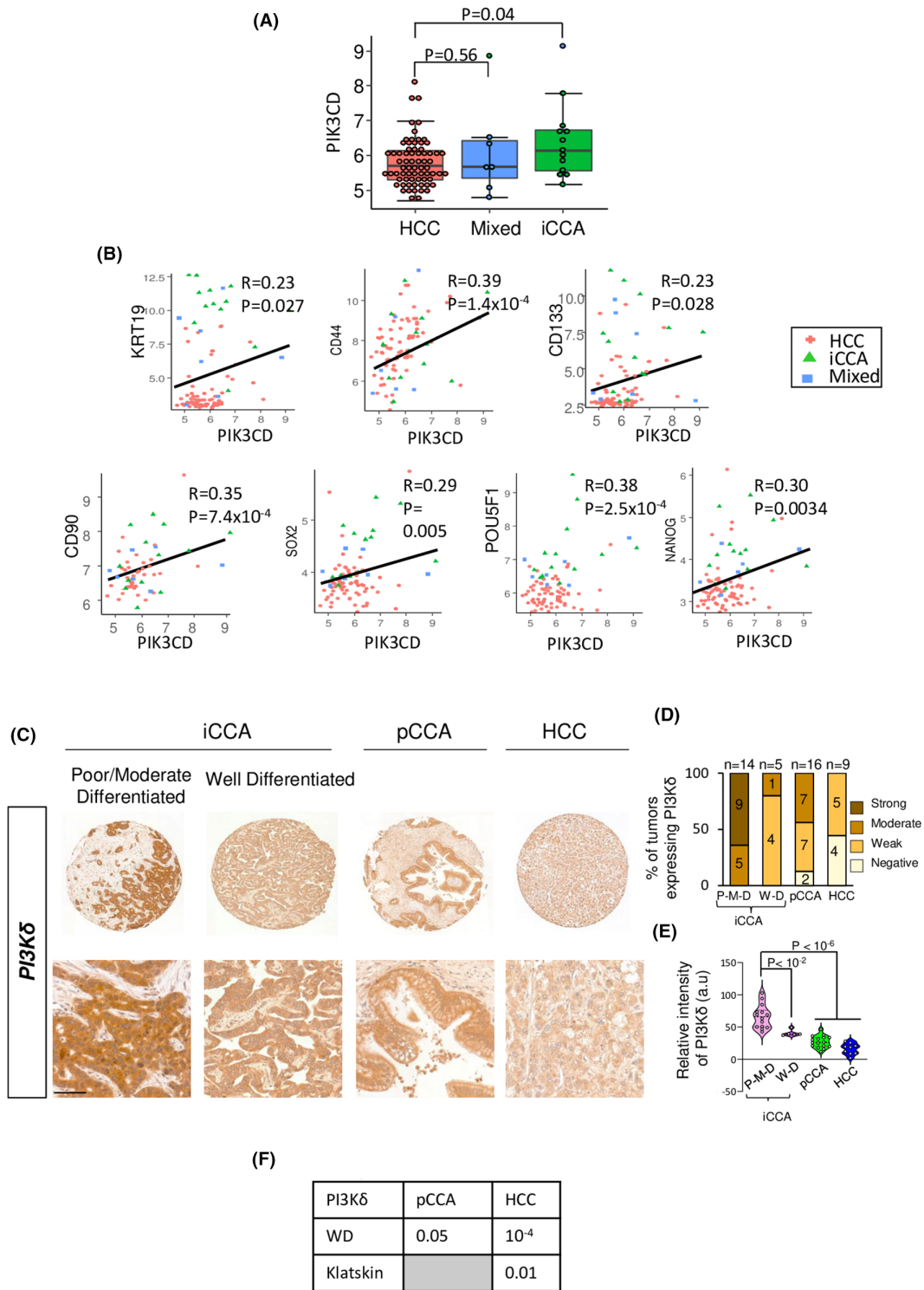


**FIGURE 1** PI3K $\delta$  is expressed at the higher level in CCA than in HCC and, increased in poor differentiated tumours and correlated to EMT in CCA. (A) Expression of PI3K $\delta$  in distinct subgroups of liver cancers: Hepatocellular carcinoma (HCC), intrahepatic cholangiocarcinoma (iCCA), mixed: HCC + iCCA. (B) Scatterplot of PI3K $\delta$  expression versus expression of distinct stem cell markers in liver cancers: KRT19, CD44, CD133, CD90, SOX2, POU5F1, NANOG. (C) Representative images of PI3K $\delta$  protein expression in liver cancer tissues using tissue microarray by immunohistochemistry. (D,E) analysis in a mix of 14 tumours poor and moderate differentiated (M-P-D) and 5 well-differentiated (W-D) intrahepatic cholangiocarcinoma (iCCA), 16 perihilar cholangiocarcinoma (pCCA) and 9 hepatocellular carcinoma (HCC). (F) Table representing the *p*-values of PI3K $\delta$  expression between the liver cancer groups corresponding to the graph. All data represented mean  $\pm$  SEM (Student's *t* test).

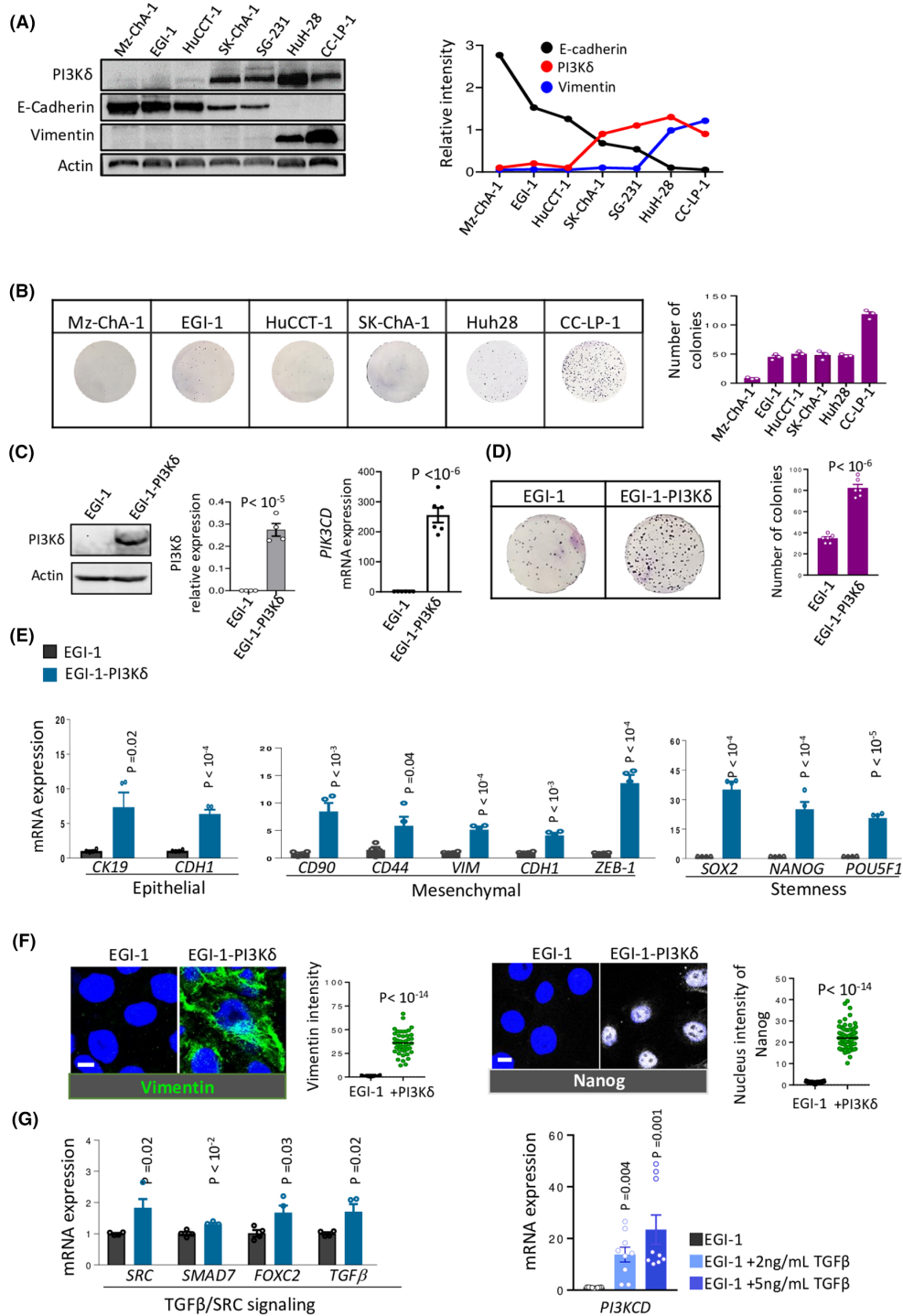


**FIGURE 2** PI3Kδ enhances CCA stemness and EMT in vitro. (A) Western blot analysis for the protein expression level of PI3Kδ, E-cadherin and Vimentin in CCA cell lines (Mz-ChA-1, EGI-1, HuCCT-1, SK-ChA-1, SG-231, Huh-28 and CC-LP-1). Quantification of PI3Kδ, E-cadherin and Vimentin relative intensity (right). Data are representative of three separate experiments. (B) Colony formation ability of CCA cell lines (Mz-ChA-1, EGI-1, HuCCT-1, SK-ChA-1, Huh-28 and CC-LP-1) cultured for 7 days. Quantification of number of colonies (right). (C) Western blot analysis for the expression level of PI3Kδ performed in EGI-1 and EGI-1-PI3Kδ cells. Quantification of PI3Kδ relative intensity (grey bars). RT-qPCR analysis of PI3Kδ expression performed in EGI-1 and EGI-1-PI3Kδ cells (right, white bars). RPLP0 was used as a housekeeping gene for normalization. (D) Colony formation ability of EGI-1 and EGI-1-PI3Kδ cells cultured for 7 days. Quantification of number of colonies (right). (E) RT-qPCR analysis of different gene expression performed in EGI-1, EGI-1-PI3Kδ cells. RPLP0 was used as a housekeeping gene for normalization. (F) RT-qPCR analysis of *SRC*, *SMAD7*, *FOXC2* and *TGFβ* expressions performed in EGI-1 and EGI-1-PI3Kδ cells and *PI3KCD* expression in EGI-1 cells were treated by two doses of TGFβ (right bars). (G) Immunofluorescence staining for vimentin (green) and Nanog (White) was performed in 2D culture of EGI-1, EGI-1-PI3Kδ. Quantification of the vimentin and Nanog intensity between the two conditions are next to the corresponding image. All data represented mean  $\pm$  SEM. (Student's *t* test).

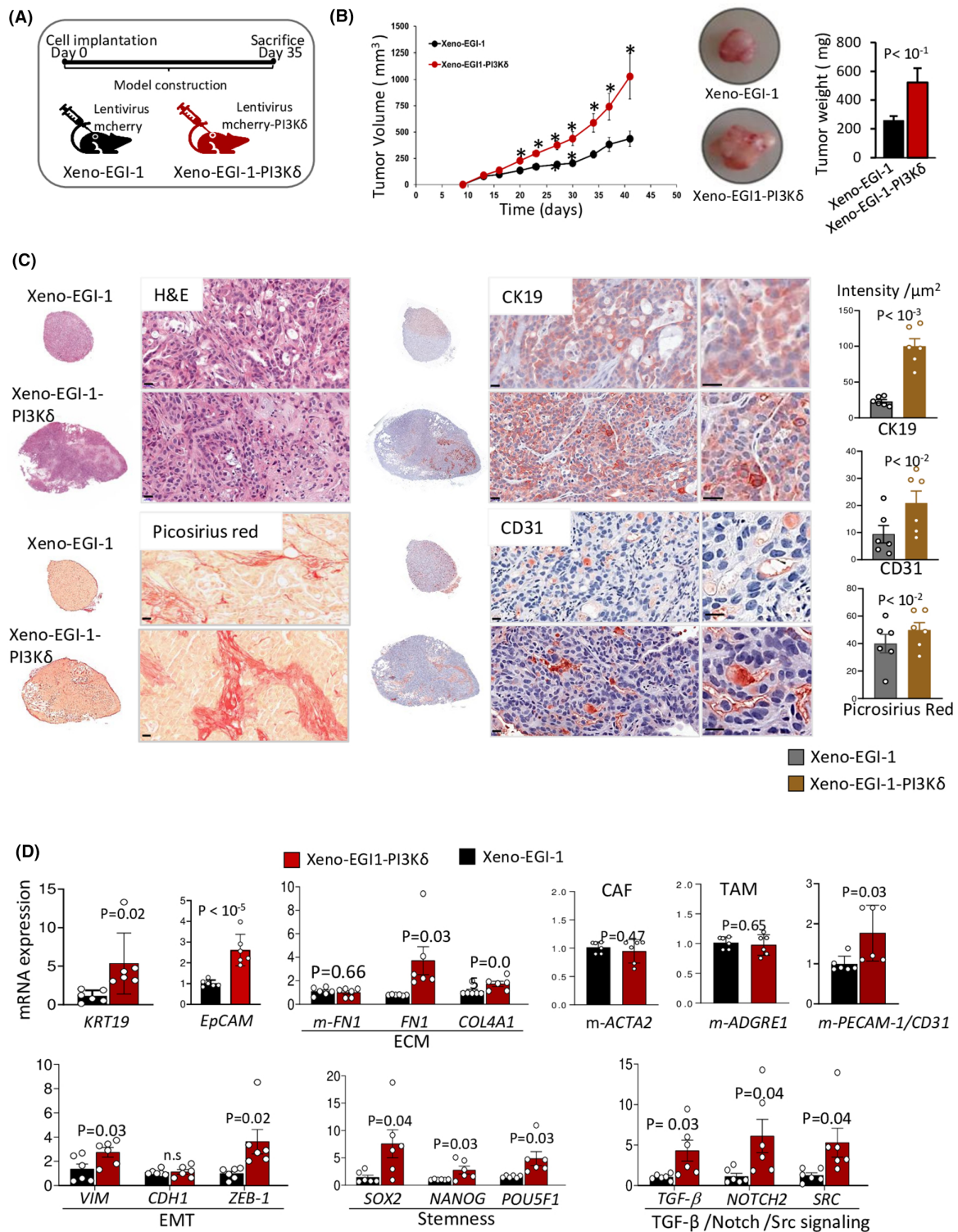


**FIGURE 3** PI3Kδ promotes tumorigenesis, fibrosis, angiogenesis and secretion of different cytokines in the CCA mouse model. (A) Schematic representation of CCA xenograft model establishment protocol. (B) Growth curves of xenograft tumours in mice bearing EGI-1 (Xeno-EG1-1) and EGI-1-PI3Kδ (Xeno-EG1-1-PI3Kδ) cells. Representative images of a tumour from the Xeno-EG1-1 and Xeno-EG1-1-PI3Kδ groups and representation of the overall tumour weight of each condition at sacrifice (right). (C) Representative haematoxylin-eosin (H&E) image of Xeno-EG1-1 and Xeno-EG1-1-PI3Kδ xenograft sections (left). Representative image of CK19, Picosirius red and CD31 staining performed in Xeno-EG1-1 and Xeno-EG1-1-PI3Kδ (right). Scale bar = 20 μm. Quantification of relative intensities of the markers (right). (D) RT-qPCR analysis of the expression of different genes performed in the Xeno-EG1-1 and Xeno-EG1-1-PI3Kδ tumours. All data represent the mean ± SEM. (Student's *t*-test).



by RT-qPCR the EMT markers and we observed that the mesenchymal markers *VIM* and *ZEB1* increased whereas no significant change was observed to the *CDH1* (Figure 3D). The pluripotency markers (*SOX2*, *POU5F1*, *NANOG*) also increased in EGI-1-PI3K $\delta$  xenograft (Figure 3D). Interestingly, TGF $\beta$ , Notch 2 and SRC increased (Figure 3D) as shown in Figure 2F and thus, strongly suggested that these signalling molecules were involved in the fibrosis and angiogenesis induced by PI3K $\delta$  expression in CCA cells.

### 3.4 | PI3K $\delta$ regulates liver fibrosis and angiogenesis in mice injected with AAV vectors

To get more insight into the role of PI3K $\delta$  in vasculature development and fibrosis, we generated AAV8-control mice and AAV8-mediated PI3K $\delta$  expression (AAV-PI3K $\delta$ ) as recently reported<sup>30</sup> (Figure 4A). The histology of AAV-control mice liver displayed normal features; in contrast, AAV-PI3K $\delta$  mice displayed a subtle ductular reaction with more numerous and disorganized small ductular structures around the portal vein (Figure 4B). Interestingly, the sinusoids were wider in the AAV-PI3K $\delta$  liver than in the AAV-control mice liver. The CD31 staining intensity (Figure 4C) and its transcripts increased (Figure 4E). There was also fibrosis enrichment (Figure 4D). Interestingly, PI3K $\delta$  overexpression in the AAV-PI3K $\delta$  liver increased EMT/stemness markers and TGF $\beta$ /Src as revealed in vitro (Figure 2F) and in xenografts (Figure 3D). Together these results confirmed that PI3K $\delta$  expression in CCA epithelial cells, controlled angiogenesis and fibrosis through TGF $\beta$ /Src signalling.

### 3.5 | PI3K $\delta$ expression promotes secretion of TGF $\beta$ and angiogenic cytokines and stimulates lymphangiogenesis

Subsequent to the effects of PI3K $\delta$  expression on fibrosis and angiogenesis and to get more insights into the involved mechanisms, we quantified human TGF $\beta$ 1 and pro-angiogenic cytokines, such as vascular endothelial growth factor-A and C (VEGF-A and -C), placental growth factor (PIGF), basic-fibroblast growth factor (bFGF) in mouse serum using multiplex assays and found that they significantly increased (Figure 5A,B). Together these data revealed that PI3K $\delta$  in human CCA cells promotes EMT/stemness and contributed to fibrosis and angiogenesis in mice through the secretion of TGF $\beta$ , VEGFs, PIGF and bFGF.

The lymphatic vasculature is important as the major routes for metastatic spread to the lymph node and significant progress has been made in the understanding of lymphangiogenesis and cancer metastasis.<sup>32</sup> The VEGF-C has been found to be the common lymph-angiogenic factor, acting predominantly via VEGF receptor-3 (VEGFR-3),<sup>33</sup> which is expressed by lymphatic endothelial cells and VEGF-C strongly promoted the growth of tumour-associated lymphatic vessels.<sup>34–36</sup> One of the major hallmarks of CCA is its lymph

node metastasis. The lymphatic invasion and lymph node involvement are important prognostic indicators for iCCA, however, lymph node metastasis and lymphangiogenesis at the mechanistic level in intrahepatic cholangiocarcinoma are poorly understood.<sup>37</sup> Thus, we investigated the lymphatic vessel by immunofluorescence staining of lymphatic endothelial cells using human lymphatic vessel endothelial hyaluronan receptor 1 (LYVE-1) antibody. First, we stained a section of xenografts from EGI-1 and EGI-1-PI3K $\delta$  cells used to stain CD31 (Figure 4). Interestingly, while the signal was low in the EGI-1 xenografts, a marked increase of LYVE-1 staining was observed in EGI-1-PI3K $\delta$  xenografts. The number and the length of vessel branches were significantly higher in EGI1-PI3K $\delta$  than in the control EGI-1 tumours (Figure 5C). Similar results were obtained by analysing the liver of AAV mice (Figure 5D). Nevertheless, the effects were not as prominent as observed with xenografts. Together these data strongly suggested a new role of CCA cell-expressed PI3K in the development of lymphatic vessels.

### 3.6 | PI3K $\delta$ expression in CCA cells promotes ECM remodelling

To further decipher the mechanism of action of PI3K $\delta$ , we used a 3D organoid model of CCA cells. This system allows polarization of the cells which form organoids/cyst structures more relevant to the in vivo conditions than the 2D culture.<sup>22</sup> Accordingly, EGI-1 and EGI-1-PI3K $\delta$  cells were cultured in 3D in Matrigel. Strikingly, EGI-1-PI3K $\delta$  cells formed cysts with open single and wide lumen visualized by actin staining while the control cells formed a mass of cells with small multi-lumens (Figure 6A,B). We also analysed the expression of PI3K $\delta$  which was almost absent in EGI-1 cells (Figure 6A) in line with the immunoblot data (Figure 2A) and strongly enriched in the basolateral membrane of EGI-1-PI3K $\delta$  cells (Figure 6A). Subsequently, we analysed the ECM components such as laminin, collagen IV and fibronectin which increased at the basement membrane around cysts formed by EGI-1-PI3K $\delta$  cells compared to EGI-1 cells (Figure 6B–D). Similar results were observed using HuCCT-1-PI3K $\delta$  cells (Figure S5). These data recalled the previously reported role of PI3K $\delta$  in lumen formation and ECM assembly using MDCK cells grown in 3D.<sup>22</sup> These data are also in line with the effects of PI3K $\delta$  in the fibrotic stroma formation in CCA xenografts (Figure 3C,D) as well as in AAV-PI3K $\delta$  mouse liver (Figure 4D).

### 3.7 | PI3K $\delta$ promotes ECM remodelling and increases Src and Notch pathways through TGF $\beta$ signalling

To further validate the contribution of TGF $\beta$  dependent mechanisms in the role of PI3K $\delta$  in CCA progression, EGI-1 and EGI-1-PI3K $\delta$  cells were grown in 3D culture and treated with SB431542, a TGF $\beta$  receptor inhibitor. After 6 days in culture, the control EGI-1 cells

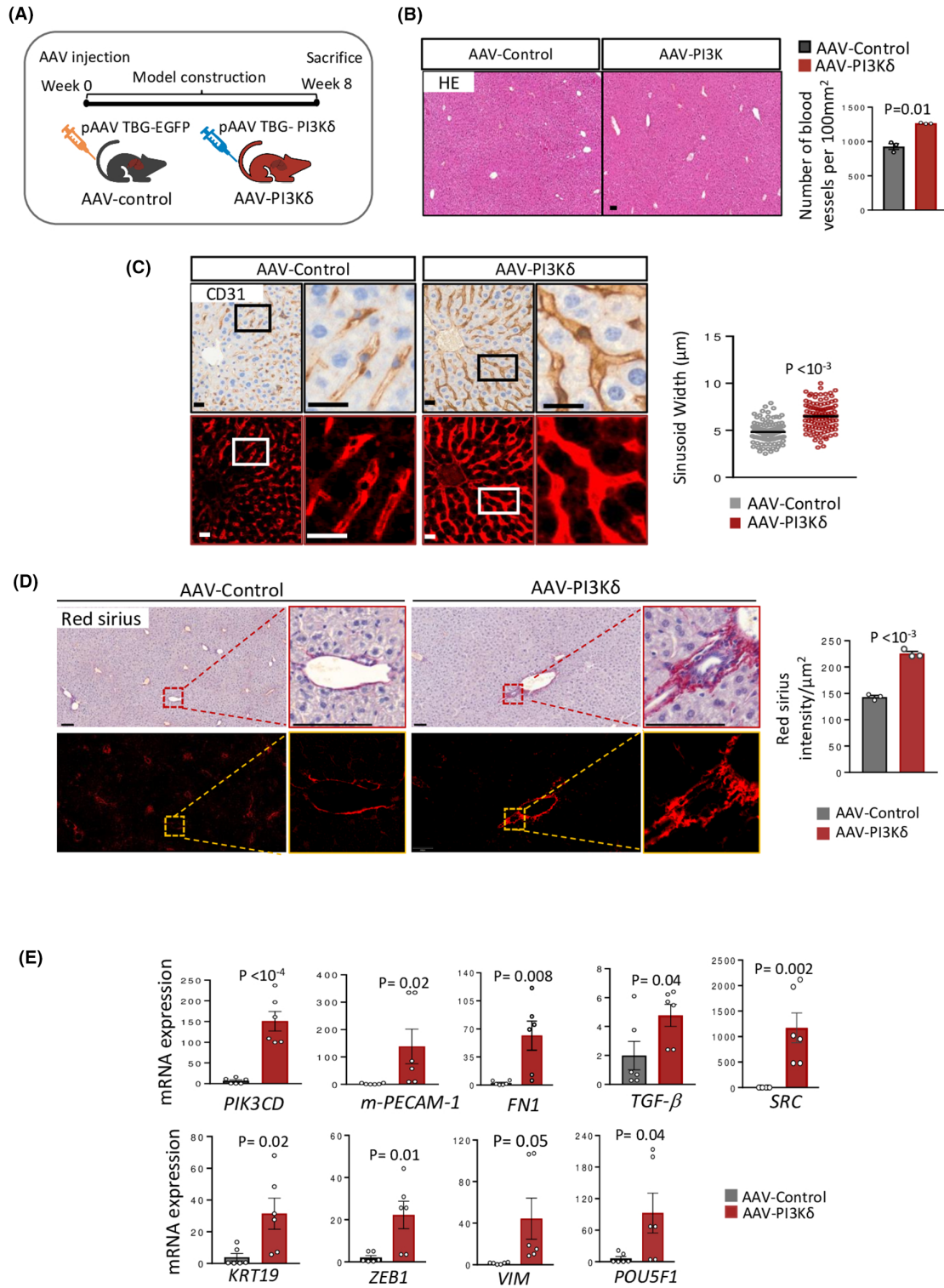


**FIGURE 4** PI3K $\delta$  promotes vascular growth and fibrosis in mice model injected with AAV vectors. (A) Schematic representation of the protocol for the establishment of the AAV-PI3K $\delta$  mice model. (B) Representative images of H&E staining of liver section from mice injected with pAAV8-TBG-EGFP (AAV-Control) and with pAAV8-TBG- PI3K $\delta$  (AAV-PI3K $\delta$ ). Scale bars=200  $\mu$ m. (C) Representative images of immunohistochemistry staining of CD31 on AAV-control and AAV-PI3K $\delta$  liver. Coloured images using CaseViewer were presented below each panel. Bar graphs representing the number of blood vessels per 100mm<sup>2</sup> and the sinusoid width (n=100) (right). (D) Representative images of Picosirius red staining on AAV-control and AAV-PI3K $\delta$  liver. Coloured images using CaseViewer were presented below each panel. Quantification of the Picosirius red intensity (right). Scale bars=100  $\mu$ m. (E) RT-qPCR analysis of different gene expression performed in liver of AAV-control and AAV-PI3K $\delta$  mice. All data represented mean  $\pm$  SEM (Student's t test).

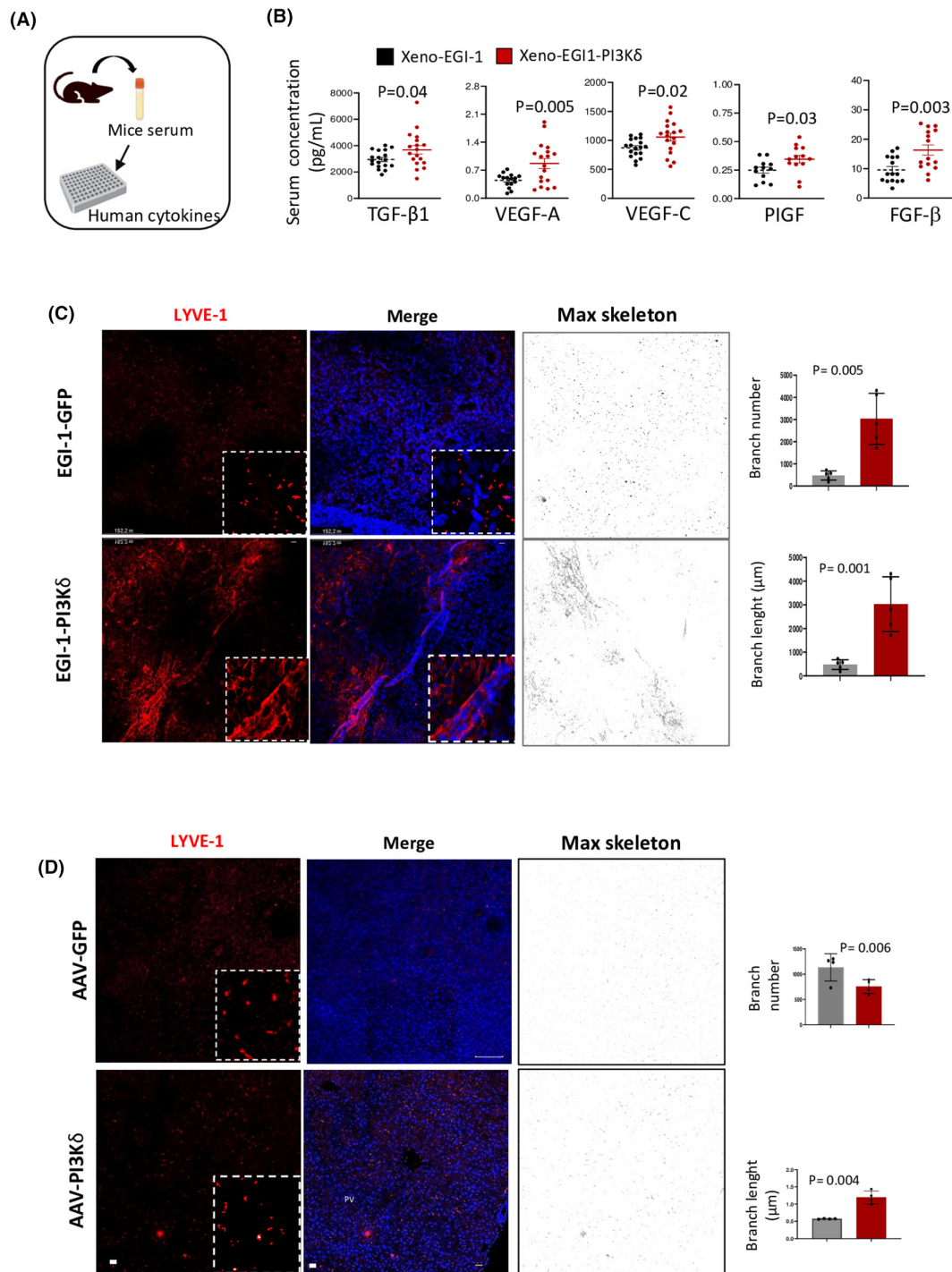


**FIGURE 5** PI3K $\delta$  expression promotes the environment for vascular development including lymph vessels. (A) Schematic representation of ELISA protocol. (B) ELISA of several cytokine/growth factors performed in the serum of Xeno-EGI-1 and Xeno-EGI-1-PI3K $\delta$  mice. All data represent the mean  $\pm$  SEM. (Student's t test). (C) Immunofluorescence staining for LYVE-1 (red) and nuclei (blue) performed in the xenograft of Xeno-EGI-1 and Xeno-EGI-1-PI3K $\delta$ . (D) Immunofluorescence staining for LYVE-1 (red) and nuclei (blue) performed in the AAV-control tissues section and AAV-PI3K $\delta$  tissues section. Quantification by LYVE-1 of the number of vessels is based on a binary image obtained by the skeleton analyses plugin of the Fiji software (branch  $n=4$  images per condition) and vessel length ( $n=800$  per condition). Scale bar = 20  $\mu$ M.

formed multi-lumen spheroids while EGI-1-PI3K $\delta$  cells displayed a central large lumen (Figure 7A,C) as described in Figure 5. Treatment of cells with SB431542, inhibited the formation of the central

lumen and the cells formed cysts with multiple lumens as seen in EGI-1 control cysts (Figure 7A,C). The treatment of EGI-1-PI3K $\delta$  cells with SB431542 significantly decreased the elevated expression

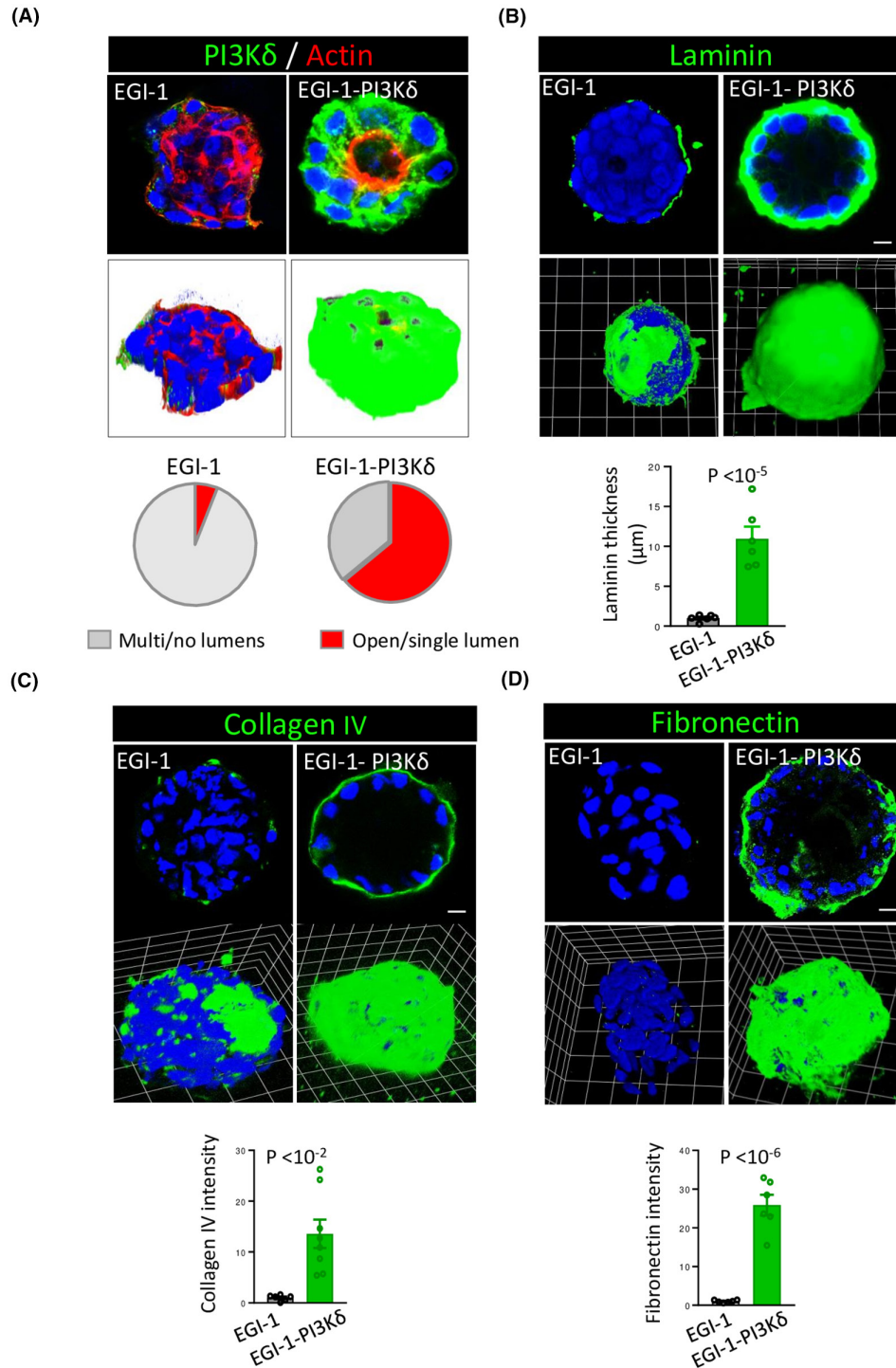


**FIGURE 6** PI3K $\delta$  expression increases lumen and ECM in EGI-1 cells. (A) Immunofluorescence staining for PI3K $\delta$  (green), F-actin (red) and nuclei (blue) performed in the organoids of EGI-1 and EGI-1-PI3K $\delta$  after 6 days of 3D culture. Quantification of the phenotypes percentage in EGI-1 and EGI-1-PI3K $\delta$  (below). (B–D) Immunofluorescence staining for laminin (green), collagen IV (green), fibronectin (green), F-actin (red) and nuclei (blue) performed in organoids. Quantification of the different markers intensity between the two conditions (below). All data represented mean  $\pm$  SEM. (Student's *t* test).

of N-cadherin, laminin, fibronectin and Src in EGI-1-PI3K $\delta$  cells (Figure 6A). Interestingly the high expression of Notch2 and Notch3 in EGI-1-PI3K $\delta$  cells was also decreased upon SB431542 treatment

(Figure 7B). Finally, we validated these data by performing RT-qPCR analyses (Figure 7D) and thus revealed the crucial role of TGF $\beta$  signalling in CCA cell-PI3K $\delta$  activities.

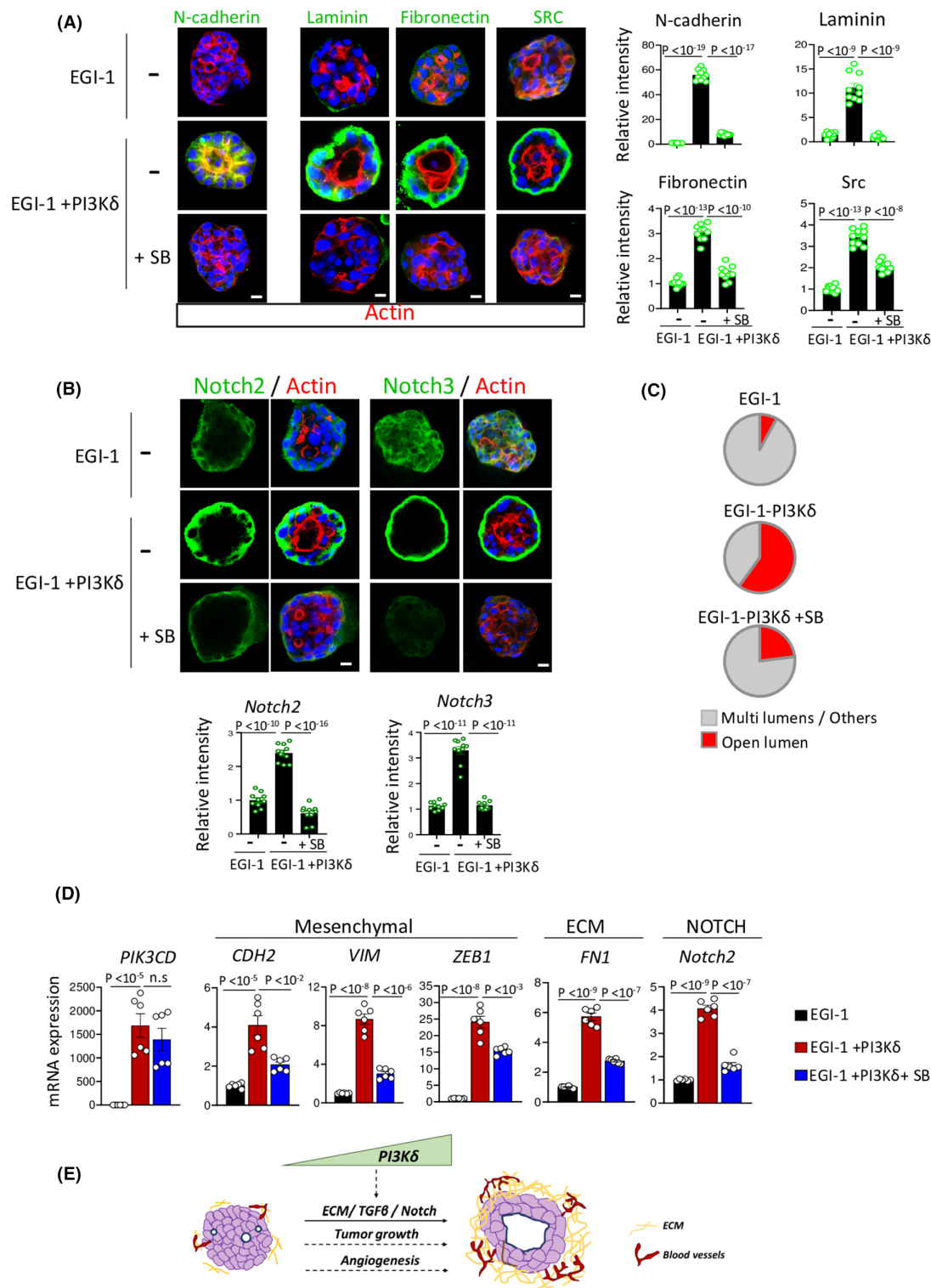


**FIGURE 7** The PI3K $\delta$ -induced ECM remodelling and increase of Notch and src depend on TGF $\beta$ . (A,B) Immunofluorescence staining for N-cadherin (green), laminin (green), fibronectin (green), src (green), Notch2 (green), Notch3 (green), F-actin (red) and nuclei (blue) performed in the organoids of EGI-1 or EGI-1-PI3K $\delta$  treated or not with TGF $\beta$  inhibitor SB431542 (2  $\mu$ M) after 6 days of 3D culture. Quantification of the different markers intensity between the conditions (right). (C) Distribution of the cysts according to their phenotypes in EGI-1, EGI-1-PI3K $\delta$  and EGI-1-PI3K $\delta$ +SB. All data represented mean  $\pm$  SEM. (Student's *t* test). (D) RT-qPCR analysis of different gene expression performed in EGI-1 or EGI-1-PI3K $\delta$  cells treated or not with 2  $\mu$ M of SB431542 for 6 days in 3D culture. (E) Schematic representation of the PI3K $\delta$ -dependant morphogenesis, ECM and angiogenesis in CCA.

### 3.8 | Combined expression of PI3K $\delta$ and the EMT marker vimentin discriminates three groups of iCCA related to cancer progression

According to our results, cancer cell-intrinsic PI3K $\delta$  could serve as a potential biomarker for CCA classification and as a driver of tumour progression. To get further insights in, we took RNA-sequencing data of 1072 cancer cell lines of CCLE collection, 26 iCCA cell lines were selected through the depmap web data portal. Combined expression of the PI3K $\delta$  gene (*PIK3CD*) and vimentin gene (*VIM*) used as an EMT marker in the iCCA cell lines revealed an important dispersion of these cell lines through the total panel of CCLE cell line collection (Figure S6A). This analysis distinguishes 3 groups of iCCA cell lines: a group (9 cell lines) named 'Low/Low' with low expression of *VIM* and *PIK3CD*, a group (7 cell line) named 'High/Low' with high expression of *VIM* and low expression of *PIK3CD* and a group (9 cell lines) named 'High/High' with high expression of both *VIM* and *PIK3CD* (Figure S6A). Total RNA-sequencing of these 26 iCCA cell lines was stratified according to the 3 *VIM-PIK3CD* subgroups to perform a supervised machine learning process through the pamr package (Figure S6B). This analysis identified 227 genes (Table S1) with a minimal misclassification error of 0.195 between groups (Figure S6C,D) and the majority of 87 genes predictor of group  $VIM^{low}/PIK3CD^{low}$ , 34 genes for group  $VIM^{high}/PIK3CD^{low}$  and 44 genes for group  $VIM^{high}/PIK3CD^{high}$  were identified (Figure S6D). Among these genes, the best 75 predictive markers allowed the stratification of the 3 groups by unsupervised clustering (Figure S6E,F). Next, the 87 genes predictive of the  $VIM^{low}/PIK3CD^{low}$  group were confirmed by unsupervised clustering (Figure S7A) and by unsupervised principal component analysis (Figure S7B). Functional enrichment performed on the GO-BP database revealed plasma membrane organization, desmosome organization, epithelial cell differentiation and cell junction organization (Figure S7C,D). Therefore, suggesting that the  $VIM^{low}/PIK3CD^{low}$  group harboured mainly epithelial cell characteristics. Besides, the 34 genes predictive of  $VIM^{high}/PIK3CD^{low}$  group were also confirmed by unsupervised clustering (Figure S8A) and by unsupervised principal component analysis (Figure S8B). Functional enrichment performed on the GO-BP database revealed the main implication of this signature in functions affecting immune humoral response and protein activation cascade like complement cascade (Figure S8C,D). Finally, the signature of 44 genes predictive of  $VIM^{high}/PIK3CD^{high}$  group was in turn confirmed by unsupervised clustering (Figure 8A) and by unsupervised principal component analysis (Figure 8B). Functional enrichment performed on the GO-BP database revealed the main implication of this signature in functions affecting the extracellular structure and organization, response to wounding and growth factors (Figure 8C,D). Altogether,  $VIM^{high}/PIK3CD^{high}$  group were characterized by genes involved in tissue remodelling affecting ECM organization and blood vessel development through response to wounding and growth factors. The best predictive markers found for these three groups of iCCA cells were

presented in Figure S9. Thus, analysis of these three groups of cell lines strongly suggested that increased PI3K $\delta$  expression in CCA cells is associated with cancer progression and aggressiveness as depicted in the Figure 8E. We proposed 3 stages of iCCA progression according to the 3 identified subgroups; in stage 1, CCA cells have epithelial features, stage 2 is characterized by humoral immune response through complement cascade and stage 3 is associated with a specific increase in PI3K $\delta$  and tissue and ECM remodelling and angiogenesis.

## 4 | DISCUSSION

In this manuscript, we demonstrated that PI3K $\delta$  contributes to the development of the desmoplastic stroma and the aggressiveness of CCA by activation of TGF $\beta$ /src/Notch signals.

We found that iCCA with moderate-to-poor differentiate tumours express more PI3K $\delta$  than well-differentiated iCCA, pCCA or HCC via investigating human liver cancer biopsies and screening databases, suggesting that high PI3K $\delta$  expression is prone to aggressiveness.

Recently we reported that a balance of PI3K $\delta$  expression is required for hepatocyte differentiation.<sup>35</sup> Indeed, its overexpression induced dedifferentiation and stemness while its inhibition in cells with low expression promoted EMT and thus distinguished these two processes.<sup>38</sup> Interestingly we obtained similar data using CCA cells (Figure 2). PI3K $\delta$  overexpression did not down-regulated the expression of epithelial molecule *CDH1* in CCA cells while increasing mesenchymal markers and pluripotency transcription factors. Thus, suggesting that the increase of PI3K $\delta$  induced an intermediate EMT-associated phenotype with stemness.<sup>38</sup> These results were validated by in vivo experiments using EGI-1-PI3K $\delta$  xenograft models (Figure 3). Together these data confirmed the larger role of PI3K $\delta$  in the regulation of plasticity/EMT beyond hepatocyte.

TGF $\beta$  family signalling maintains the pluripotency and the self-renewal of stem cells<sup>39</sup> and are key inducers of the EMT process.<sup>40</sup> TGF $\beta$  overexpression leads to CCA tumorigenesis and metastasis.<sup>41</sup> Furthermore our recent work demonstrated that PI3K $\delta$  activity discriminates EMT and stemness based on distinct TGF $\beta$  signalling in malignant hepatocytes.<sup>30</sup> Interestingly in this study our results showed that PI3K $\delta$  expression in CCA cells increased TGF $\beta$  expression both in vitro 3D cultures and in vivo. Particularly PI3K $\delta$  expression in CCA cells promoted secretion of TGF $\beta$  and angiogenic factors such as VEGF and bFGF in the serum of xenograft mice (Figure 5). The most striking feature of PI3K $\delta$  overexpression is ECM deposition as exemplified by our precedent report,<sup>22</sup> and the data presented in Figure 6 using EGI-1 cells. Moreover, PI3K $\delta$  overexpression increased src kinase, a regulator of ECM organization whose activation is also dependent on TGF $\beta$  signalling<sup>38</sup> (Figures 2, 3 and 7). Accordingly, we showed that PI3K $\delta$ -dependent ECM remodelling and expression of EMT markers are dependent on TGF $\beta$  signalling (Figure 7). Together these studies revealed that

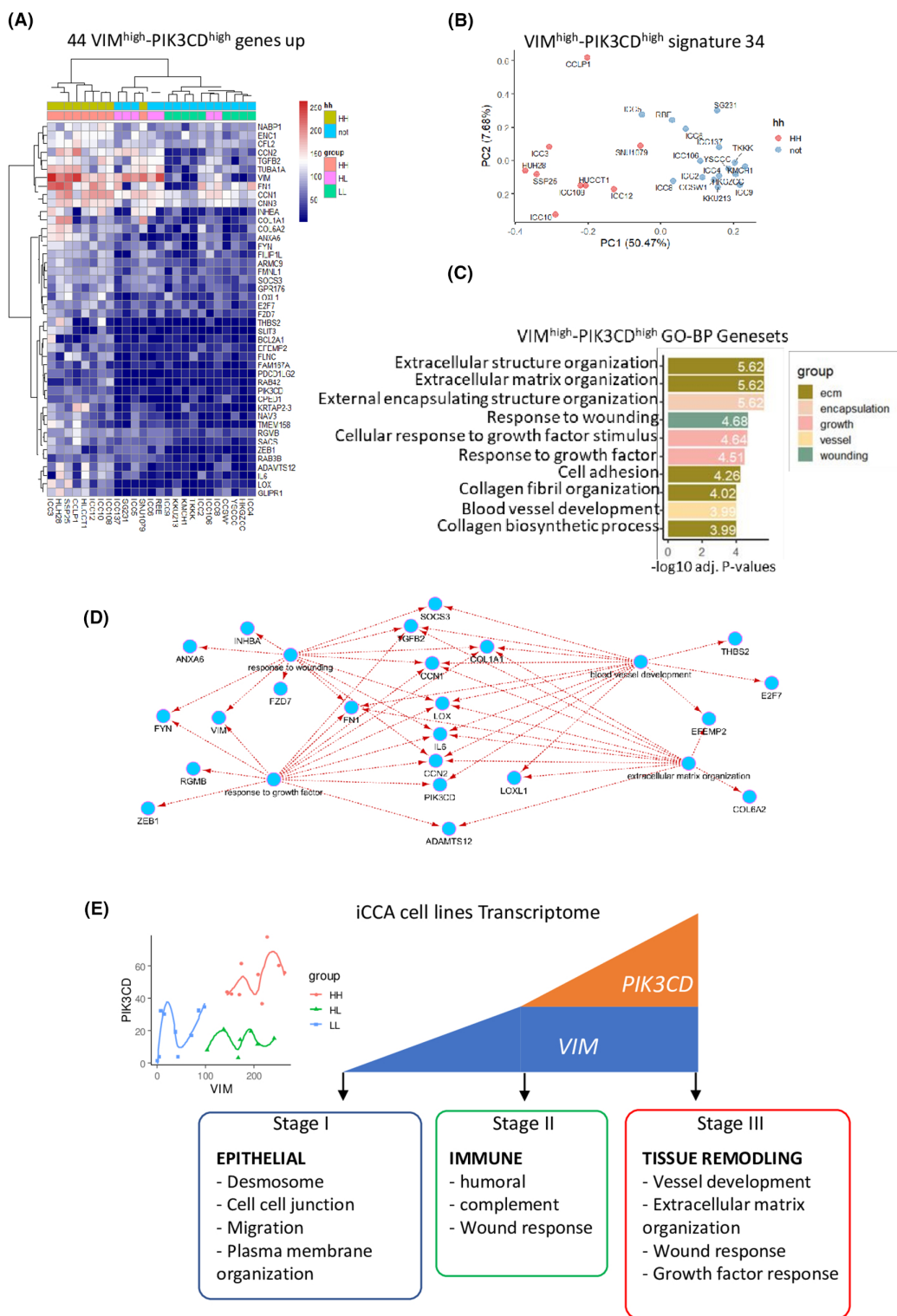


**FIGURE 8** Biological process features of  $VIM^{high}/PIK3CD^{high}$  CCA group. (A) Expression heatmap based on 44 predictive markers for  $VIM^{high}/PIK3CD^{high}$  (HH) iCCA cell line subgroup. (B) Unsupervised principal component analysis validating HH iCCA cell line signature. (C) Barplot of functional enrichment performed on Gene Ontology Biological Process (GO-BP) database. (D) Functional enrichment network of HH subclass signature. (E) Synopsis of the graphical abstract. Whole transcriptome analysis of the CCLE cancer cell line encyclopedia allowed to stratified iCCA cell lines into three distinct groups based on alternative expression of  $VIM$  and  $PIK3CD$ . iCCA cell line stage I with both low expression of  $VIM$  and  $PIK3CD$  was characterized by activation of epithelial cell structure activation like cell–cell junction through desmosome. iCCA cell line stage II with high expression of  $VIM$  and low expression of  $PIK3CD$  is characterized by activation of humoral immune response through complement cascade activation. iCCA cell line stage III with both high expression of  $VIM$  and  $PIK3CD$  is characterized by activation of tissue remodelling criteria like extracellular matrix structure and organization and blood vessel development through response to wounding and growth factors.

*PI3Kδ* promotes stemness and fibrosis in CCA via TGFβ activation. The CAFs are a key component of the tumour microenvironment which could also contribute to ECM remodelling, fibrosis and EMT.<sup>42</sup> As a result, we analysed in xenografts the transcripts of αSMA and F4/80 used to quantify CAFs and tumour-associated macrophages (TAM) respectively. However, no significant changes were observed for both transcripts (Figure 3D). Subsequently, we proposed that the increased fibrosis in xenografts is induced by PI3Kδ expressed in CCA cells. However, we could not exclude the participation of CAFs which need further investigations. The assessment of tumour necrosis is considered as a valuable additional prognostic indicator in CCA and increased necrosis in tumour was correlated to reduced recurrence-free and overall survival.<sup>43</sup> Notably, all tumours with PI3Kδ expression showed necrosis (Figure S4B). Together these data supported the association of PI3Kδ expression with poor prognosis in CCA.

Importantly, our study, also revealed that overexpression of PI3Kδ in CCA epithelial cells promoted vasculature development, angiogenesis and lymphangiogenesis (Figures 3–5). We also showed that PI3Kδ enriched-CCA cells secreted angiogenic factors in mouse serum (Figure 5). Hence, we proposed that these secreted cytokines could largely contribute to angiogenesis by recruitment of endothelial cells. This hypothesis is supported by the human origin of the secreted cytokines. This is an unprecedented description of the role of cancer cells' intrinsic *PI3Kδ* contribution to angiogenesis. Thus, PI3K played a crucial role in tubulogenesis as exemplified by enlarged lumens observed in EG11-PI3Kδ cells grown in 3D (Figures 6 and 7) which is also important for vasculature development. This activity of CCA cell intrinsic-PI3Kδ is different from the reported role of endothelial cells expressed-PI3Kδ in angiogenesis.<sup>44,45</sup>

Through whole transcriptome analysis, we classified 26 CCA cell lines according to *PIK3CD* and *VIM* expressions. We discovered three groups corresponding to three tumour development stages (Figure 8). Indeed, low *PIK3CD* and *VIM* expressions characterized stage I and cells displayed epithelial properties; in stage II, cells were characterized by humoral immune response. Therefore, approaches to immune inhibition may be proposed as an effective treatment. The *VIM* and *PIK3CD* levels were high in stage III, and the processes associated were tissue remodelling to affect ECM organization and blood cell development through wounding and growth factors. Here the *PI3Kδ* inhibitors and anti-angiogenic factors may provide effective treatment.

In conclusion, this work highlighted the detrimental effects of highly expressed PI3Kδ in CCA. These effects manifested by induction of hybrid EMT/stemness, ECM accumulation and angiogenesis regulated by TGFβ/src/Notch signalling as presented in Figure 6E. Detecting PI3Kδ with vimentin levels may be a potential diagnostic tool to classify CCA severity and help the establishment of precision medical strategies in the clinic. Hence targeting PI3Kδ using its specific approved inhibitor CAL-101 or combined with immunotherapies may represent a promising therapy for aggressive cancers with stem cells and poor survival such as CCA.

## AUTHOR CONTRIBUTIONS

Conceptualization and design: Ama Gassama-Diagne. Data generation: Vanessa Bou Malham, Nassima Benzoubir, Javier Vaquero, Christophe Desterke, Jean Agnetti, Pei Xuan Song, Ester Gonzalez-Sanchez, Ander Arbelaz, Sophie Jacques, Emanuel Di Valentin, Souad Rahmouni and Tuan Zea Tan. Data analysis and interpretation: Vanessa Bou Malham, Nassima Benzoubir, Javier Vaquero, Christophe Desterke, Jean Agnetti, Mylène Sebah, Pei Xuan Song, Tuan Zea Tan, Laura Fouassier and Ama Gassama-Diagne. Manuscript preparation: Vanessa Bou Malham, Nassima Benzoubir, Javier Vaquero, Christophe Desterke, Mylène Sebah, Laura Fouassier, Didier Samuel and Ama Gassama-Diagne. Review and editing: Vanessa Bou Malham, Nassima Benzoubir, Javier Vaquero, Christophe Desterke, Mylène Sebah, Jean Agnetti, Pei Xuan Song, Ester Gonzalez-Sanchez, Ander Arbelaz, Sophie Jacques, Emanuel Di Valentin, Souad Rahmouni, Tuan Zea Tan, Jean Paul Thierry, Didier Samuel, Laura Fouassier and Ama Gassama-Diagne.

## ACKNOWLEDGMENTS

We acknowledge Larbi Amazit for assistance at the imaging core facility (UMS44, Hôpital Paul Brousse, France). We also thank Veronique Bruna, Marie-Jose Redon, Stéphanie Goujon, Olivier Trassard for their technical contribution, all in the Department of Pathology, Bicetre Hospital, Le Kremlin-Bicêtre, France. We acknowledge Sylvie Fabrega from the 'Plateforme Vecteurs Viraux et Transfert de gènes (VVTG)', Faculté de Santé Paris Centre, Université Paris Cité, for the production of lentivirus.

## FUNDING INFORMATION

VBM was supported by A.S.C. s.a.r.l, Liban, LF receives financial support from ITMO Cancer of Aviesan within the 2021–2030 Cancer Control Strategy framework on funds administered by Inserm, INCa\_16428, ANR-17-CE14-0013-01 and belongs to a team supported by the Fondation pour la Recherche Médicale (Equipe FRM 2020 no. EQU202003010517). AA is supported by the Fondation pour la Recherche Médicale (FRM SPF201809007054) and by Les Entreprises contre le Cancer Paris – Île-de-France (GEFLUC\_2019). JV is the recipient of the following postdoctoral fellowships from the Spanish Association for the Study of the Liver (AEEH), the Fondation ARC (PDF2014601431) and the LABEX PLAS@PAR (Reference ANR-11-IDEX-0004-02). JV was funded by the Spanish Ministry for Science and Innovation (MCIN: 'Ramón y Cajal' Program RYC2021-034121-I). JV, EGS and LF are members of the European Network for the Study of Cholangiocarcinoma (ENSCCA) and participate in the initiative COST action EURO-CHOLANGIO-NET (CA18122). AGD is supported by funding from the La Ligue contre le Cancer.

## CONFLICT OF INTEREST STATEMENT







The authors declare no competing interests.

## DATA AVAILABILITY STATEMENT

The data that support the findings of this study are openly available in CCLE at <https://sites.broadinstitute.org/ccle/>, reference number CCLE.



## ORCID

Vanessa Bou Malham  <https://orcid.org/0000-0002-8964-8705>  
 Ester Gonzalez-Sanchez  <https://orcid.org/0000-0002-9636-9624>  
 Didier Samuel  <https://orcid.org/0000-0001-9481-3616>  
 Mylène Sebah  <https://orcid.org/0000-0002-6122-2542>  
 Laura Fouassier  <https://orcid.org/0000-0001-6377-5610>  
 Ama Gassama-Diagne  <https://orcid.org/0000-0002-9878-7811>

## REFERENCES

- Seehawer M, D'Artista L, Zender L. The worst from both worlds: cHCC-ICC. *Cancer Cell*. 2019;35(6):823-824.
- Banales JM, Marin JGG, Lamarca A, et al. Cholangiocarcinoma 2020: the next horizon in mechanisms and management. *Nat Rev Gastroenterol Hepatol*. 2020;17(9):557-588.
- Müsch A. From a common progenitor to distinct liver epithelial phenotypes. *Curr Opin Cell Biol*. 2018;54:18-23.
- Raven A, Lu WY, Man TY, et al. Cholangiocytes act as facultative liver stem cells during impaired hepatocyte regeneration. *Nature*. 2017;547(7663):350-354.
- Sia D, Villanueva A, Friedman SL, Llovet JM. Liver cancer cell of origin, molecular class, and effects on patient prognosis. *Gastroenterology*. 2017;152(4):745-761.
- Nieto MA, Huang RYJ, Jackson RA, Thiery JP. EMT: 2016. *Cell*. 2016;166(1):21-45.
- Pei D, Shu X, Gassama-Diagne A, Thiery JP. Mesenchymal-epithelial transition in development and reprogramming. *Nat Cell Biol*. 2019;21(1):44-53.
- Hepburn AC, Steele RE, Veeratterapillay R, et al. Correction: the induction of core pluripotency master regulators in cancers defines poor clinical outcomes and treatment resistance. *Oncogene*. 2019;38(22):4425.
- Shibue T, Weinberg RA. EMT, CSCs, and drug resistance: the mechanistic link and clinical implications. *Nat Rev Clin Oncol*. 2017;14(10):611-629.
- Fruman DA, Chiu H, Hopkins BD, Bagrodia S, Cantley LC, Abraham RT. The PI3K pathway in human disease. *Cell*. 2017;170(4):605-635.
- Bilanges B, Posor Y, Vanhaesebroeck B. PI3K isoforms in cell signaling and vesicle trafficking. *Nat Rev Mol Cell Biol*. 2019;20(9):515-534.
- Guillemet-Guibert J, Bjorklof K, Salpekar A, et al. The p110 $\beta$  isoform of phosphoinositide 3-kinase signals downstream of G protein-coupled receptors and is functionally redundant with p110 $\gamma$ . *Proc Natl Acad Sci USA*. 2008;105(24):8292-8297.
- Chantry D, Vojtek A, Kashishian A, et al. p110delta, a novel phosphatidylinositol 3-kinase catalytic subunit that associates with p85 and is expressed predominantly in leukocytes. *J Biol Chem*. 1997;272(31):19236-19241.
- Furman RR, Sharman JP, Coutre SE, et al. Idelalisib and rituximab in relapsed chronic lymphocytic leukemia. *N Engl J Med*. 2014;370(11):997-1007.
- Gopal AK, Kahl BS, de Vos S, et al. PI3K $\delta$  inhibition by Idelalisib in patients with relapsed indolent lymphoma. *N Engl J Med*. 2014;370(11):1008-1018.
- Goulielmaki E, Bermudez-Brito M, Andreou M, et al. Pharmacological inactivation of the PI3K p110 $\delta$  prevents breast tumour progression by targeting cancer cells and macrophages. *Cell Death Dis*. 2018;9(6):1-15.
- Sawyer C, Sturge J, Bennett DC, et al. Regulation of breast cancer cell chemotaxis by the phosphoinositide 3-kinase p110delta. *Cancer Res*. 2003;63(7):1667-1675.
- Park GB, Kim D. Insulin-like growth factor-1 activates different catalytic subunits p110 of PI3K in a cell-type-dependent manner to induce lipogenesis-dependent epithelial-mesenchymal transition through the regulation of ADAM10 and ADAM17. *Mol Cell Biochem*. 2018;439(1-2):199-211.
- Yue D, Sun X. Idelalisib promotes Bim-dependent apoptosis through AKT/FoxO3a in hepatocellular carcinoma. *Cell Death Dis*. 2018;9(10):935.
- Ko E, Seo HW, Jung ES, et al. PI3K $\delta$  is a therapeutic target in hepatocellular carcinoma. *Hepatology*. 2018;68(6):2285-2300.
- Sirica AE, Gores GJ. Desmoplastic stroma and cholangiocarcinoma: clinical implications and therapeutic targeting. *Hepatology*. 2014;59(6):2397-2402.
- Peng J, Awad A, Sar S, et al. Phosphoinositide 3-kinase p110 $\delta$  promotes lumen formation through the enhancement of apico-basal polarity and basal membrane organization. *Nat Commun*. 2015;6:5937.
- Emi N, Friedmann T, Yee JK. Pseudotype formation of murine leukemia virus with the G protein of vesicular stomatitis virus. *J Virol*. 1991;65(3):1202-1207.
- Ghandi M, Huang FW, Jané-Valbuena J, et al. Next-generation characterization of the cancer cell line encyclopedia. *Nature*. 2019;569(7757):503-508.
- Tarazona S, Furió-Tarí P, Turrà D, et al. Data quality aware analysis of differential expression in RNA-seq with NOISeq R/bioc package. *Nucleic Acids Res*. 2015;43(21):e140.
- Tibshirani R, Hastie T, Narasimhan B, Chu G. Diagnosis of multiple cancer types by shrunken centroids of gene expression. *Proc Natl Acad Sci USA*. 2002;99(10):6567-6572.
- Chen J, Bardes EE, Aronow BJ, Jegga AG. ToppGene Suite for gene list enrichment analysis and candidate gene prioritization. *Nucleic Acids Res*. 2009;37(Web Server issue):W305-W311.
- Ashburner M, Ball CA, Blake JA, et al. Gene ontology: tool for the unification of biology. The Gene Ontology Consortium. *Nat Genet*. 2000;25(1):25-29.
- Cline MS, Smoot M, Cerami E, et al. Integration of biological networks and gene expression data using Cytoscape. *Nat Protoc*. 2007;2(10):2366-2382.
- Agnetti J, Bou Malham V, Desterke C, et al. PI3K $\delta$  activity controls plasticity and discriminates between EMT and stemness based on distinct TGF $\beta$  signaling. *Commun Biol*. 2022;5(1):740.
- Dos Santos A, Court M, Thiers V, et al. Identification of cellular targets in human intrahepatic Cholangiocarcinoma using laser microdissection and accurate mass and time tag proteomics\*. *Mol Cell Proteomics*. 2010;9(9):1991-2004.
- Stacker SA, Achen MG, Jussila L, Baldwin ME, Alitalo K. Lymphangiogenesis and cancer metastasis. *Nat Rev Cancer*. 2002;2(8):573-583.
- He Y, Rajantie I, Pajusola K, et al. Vascular endothelial cell growth factor receptor 3-mediated activation of lymphatic endothelium is crucial for tumor cell entry and spread via lymphatic vessels. *Cancer Res*. 2005;65(11):4739-4746.
- Skobe M, Hawighorst T, Jackson DG, et al. Induction of tumor lymphangiogenesis by VEGF-C promotes breast cancer metastasis. *Nat Med*. 2001;7(2):192-198.
- Karpanen T, Egeblad M, Karkkainen MJ, et al. Vascular endothelial growth factor C promotes tumor lymphangiogenesis and intralymphatic tumor growth. *Cancer Res*. 2001;61(5):1786-1790.
- Mandriota SJ, Jussila L, Jeltsch M, et al. Vascular endothelial growth factor-C-mediated lymphangiogenesis promotes tumour metastasis. *EMBO J*. 2001;20(4):672-682.
- Aishima S, Nishihara Y, Iguchi T, et al. Lymphatic spread is related to VEGF-C expression and D2-40-positive myofibroblasts in intrahepatic cholangiocarcinoma. *Mod Pathol*. 2008;21(3):256-264.
- Agnetti J, Bou Malham V, Desterke C, et al. PI3K $\delta$  activity controls plasticity and discriminates between EMT and stemness based on distinct TGF $\beta$  signaling. *Commun Biol*. 2022;5(1):1-15.
- Watabe T, Miyazono K. Roles of TGF-beta family signaling in stem cell renewal and differentiation. *Cell Res*. 2009;19(1):103-115.
- Sato M, Muragaki Y, Saika S, Roberts AB, Ooshima A. Targeted disruption of TGF-beta1/Smad3 signaling protects against renal

tubulointerstitial fibrosis induced by unilateral ureteral obstruction. *J Clin Invest*. 2003;112(10):1486-1494.

41. Huang CK, Aihara A, Iwagami Y, et al. Expression of transforming growth factor  $\beta$ 1 promotes cholangiocarcinoma development and progression. *Cancer Lett*. 2016;380(1):153-162.
42. Sahai E, Astsaturov I, Cukierman E, et al. A framework for advancing our understanding of cancer-associated fibroblasts. *Nat Rev Cancer*. 2020;20(3):174-186.
43. Atanasov G, Schierle K, Hau HM, et al. Prognostic significance of tumor necrosis in hilar cholangiocarcinoma. *Ann Surg Oncol*. 2017;24(2):518-525.
44. Hirsch E, Ciraolo E, Franco I, Ghigo A, Martini M. PI3K in cancer-stroma interactions: bad in seed and ugly in soil. *Oncogene*. 2014;33(24):3083-3090.
45. Wu W, Zhou G, Han H, et al. PI3K $\delta$  as a novel therapeutic target in pathological angiogenesis. *Diabetes*. 2020;69(4):736-748.

## SUPPORTING INFORMATION

Additional supporting information can be found online in the Supporting Information section at the end of this article.

**How to cite this article:** Bou Malham V, Benzoubir N, Vaquero J, et al. Intrinsic cancer cell phosphoinositide 3-kinase  $\delta$  regulates fibrosis and vascular development in cholangiocarcinoma. *Liver Int*. 2023;00:1-18. doi:[10.1111/liv.15751](https://doi.org/10.1111/liv.15751)